Using Near-Ground Storm Relative Helicity in Supercell Tornado Forecasting

BRICE E. COFFER AND MATTHEW D. PARKER

Department of Marine, Earth, and Atmospheric Sciences, North Carolina State University, Raleigh, North Carolina

RICHARD L. THOMPSON, BRYAN T. SMITH, AND RYAN E. JEWELL

NOAA/NWS/NCEP/Storm Prediction Center, Norman, Oklahoma

(Manuscript received 7 June 2019, in final form 22 July 2019)

ABSTRACT

This study examines the possibility that supercell tornado forecasts could be improved by utilizing the storm-relative helicity (SRH) in the lowest few hundred meters of the atmosphere (instead of much deeper layers). This hypothesis emerges from a growing body of literature linking the near-ground wind profile to the organization of the low-level mesocyclone and thus the probability of tornadogenesis. This study further addresses the ramifications of near-ground SRH to the skill of the significant tornado parameter (STP), which is probably the most commonly used environmental indicator for tornadic thunderstorms. Using a sample of 20 194 severe, right-moving supercells spanning a 13-yr period, sounding-derived parameters were compared using forecast verification metrics, emphasizing a high probability of detection for tornadic supercells while minimizing false alarms. This climatology reveals that the kinematic components of environmental profiles are more skillful at discriminating significantly tornadic supercells from severe, nontornadic supercells than the thermodynamic components. The effective-layer SRH has by far the greatest forecast skill among the components of the STP, as it is currently defined. However, using progressively shallower layers for the SRH calculation leads to increasing forecast skill. Replacing the effective-layer SRH with the 0–500 m AGL SRH in the formulation of STP increases the number of correctly predicted events by 8% and decreases the number of missed events and false alarms by 18%. These results provide promising evidence that forecast parameters can still be improved through increased understanding of the environmental controls on the processes that govern tornado formation.

1. Introduction

Proximity soundings of nontornadic and tornadic severe thunderstorm environments have greatly improved our ability to forecast supercells that produce tornadoes, particularly significant tornadoes (those rated EF2 or greater). As reviewed by Johns and Doswell (1992), the use of proximity soundings for predicting the probability of severe weather dates back to the 1940s and 1950s, with renewed interest from the 1990s onward (e.g., Rasmussen and Blanchard 1998; Rasmussen 2003; Craven et al. 2004). The environmental proxies/ingredients currently used operationally to diagnose the probability of tornadogenesis originate from large datasets of proximity soundings derived from model analysis data (Thompson et al. 2003, 2007, 2012), which provide superior temporal and spatial resolution compared to that of the upper-air observing network.

The significant tornado parameter (STP) was developed as one of these tools to aid operational forecasters in the tornado forecasting process (Thompson et al. 2003), and it is probably the most widely used environmental proxy for tornadic thunderstorms. This multiple ingredient, composite index combines forecasting proxies that are known to be favorable for supercell thunderstorms and specifically tornadic supercells. The original formulation by Thompson et al. (2003) used a fixed layer calculation of storm-relative helicity (SRH; Davies-Jones et al. 1990) through the 0–1-km layer above ground level (AGL), in addition to mixed-layer (ML) convective available potential energy (CAPE), height of the lifted condensation level (LCL), and the

Supplemental information related to this paper is available at the Journals Online website: https://doi.org/10.1175/WAF-D-19-0115.s1.

Corresponding author: Brice Coffer, becoffer@ncsu.edu

DOI: 10.1175/WAF-D-19-0115.1

0–6-km bulk wind difference (6BWD). Colloquially, since 2005, this version of the STP has been referred to as the fixed-layer significant tornado parameter (STPfix). Since then, STPfix has been updated[1] to instead use the surface-based (SB) parcel for CAPE and LCL calculations, in addition to a convective inhibition (CIN) penalty. The current formulation of the STP,[2] as of March 2005, uses the effective storm inflow layer and effective storm depth for calculations of SRH (ESRH) and bulk wind difference (EBWD), respectively (Thompson et al. 2007). The concept of the effective inflow layer/storm depth is to estimate the layers that actually possess CAPE (without excessive values of CIN) within the storm's inflow. In doing so, STP eliminates cases that are not surface-based (although some supercells in seemingly 'elevated' environments can be surface-based and capable of producing severe weather; Nowotarski et al. 2011; Coffer and Parker 2015; MacIntosh and Parker 2017). The use of the effective inflow layer also allows for a more meaningful SRH calculation for elevated thunderstorms in the supercell composite parameter (SCP) by omitting layers in a sounding that are unlikely to contribute to storm updraft maintenance.

Perhaps the most impactful change from the fixed version of STP to the effective layer STP was the expansion of the depth of the SRH calculation (from the original 0–1-km layer). The depth of the effective inflow layer varies depending on the individual profile but is most often between 1250 and 2250 m AGL for right-moving supercells (Thompson et al. 2007, see their Fig. 7). One of the reasons for this change, according to Thompson et al. (2007), was due to "a concern with the previous numerical simulations and subsequent observational investigations. . .that SRH calculations have been tied to somewhat arbitrary layers AGL".

However, a growing body of literature has highlighted the importance of the near-ground shear to the eventual organization of the low-level mesocyclone and probability of tornadogenesis. From observational studies in the late 1990s and early to mid-2000s, a consensus emerged that the characteristics of the wind profile in the lower troposphere (~0–1 km AGL) are important to the probability of tornadogenesis (e.g., Markowski et al. 1998b, 2003; Rasmussen and Blanchard 1998; Rasmussen 2003; Monteverdi et al. 2003; Thompson et al. 2003; Craven et al. 2004). These proximity sounding studies indicated that the bulk lower-tropospheric wind shear is higher in environments that support tornadic storms, and that SRH concentrated near the ground favors significant tornadoes.

Simulations of convective storms have further emphasized the role of near-ground hodograph shape in the tornadogenesis process. Wicker (1996) demonstrated that environments with lower-tropospheric streamwise horizontal vorticity are more favorable than environments with lower-tropospheric crosswise horizontal vorticity for the development of near-surface vertical vorticity. Thompson and Edwards (2000), Miller (2006), and Esterheld and Giuliano (2008) provided observational evidence that "sickle shaped" hodographs (where a sharp, ~90° clockwise turn of the shear over a short vertical distance results in a kink in the hodograph) and their associated streamwise vorticity were prominent in a number of significant tornado events. Webster et al. (2014) further examined the idea that these sickle shapes are prolific tornado producers and found that, in environments characterized by sickle-shaped hodographs, mesocyclones exhibited much higher circulation than quarter-circle or straight hodograph environments. Moreover, Nowotarski and Jensen (2013) showed that, when using statistical techniques to group hodograph shapes, environments with predominately crosswise horizontal vorticity are typically associated with nontornadic supercells.

Results from the second Verification of the Origins of Rotations in Tornadoes Experiment project (VORTEX2) in 2009–10 (Wurman et al. 2012) provided further motivation for the use of near-ground SRH as an effective forecasting tool. Using the 12 best sampled supercells from VORTEX2, Parker (2014) composited 134 near-storm soundings into nontornadic and tornadic inflow soundings. Both VORTEX2 composite profiles reflected high-end supercell scenarios and were seemingly favorable for tornadoes. Each profile had a STP value near (or greater than) the climatological median for EF3+ tornadoes (Thompson et al. 2012). The most noticeable difference between the nontornadic and tornadic composites was in the lower-tropospheric wind profile; specifically, the tornadic cases had much more streamwise (and much less crosswise) horizontal vorticity in the lowest 500 m AGL. The 0–500-m SRH was twice as high in the tornadic VORTEX2 composite compared to the nontornadic composite (159 vs 80 $m^2 s^{-1}$, respectively). In contrast, it is interesting that the SRH in the (deeper) effective inflow layer was actually slightly lower in the tornadic VORTEX2 composite than the nontornadic (297 vs 314 $m^2 s^{-1}$, respectively).

[1] Current formulations of all parameters can be found in the help sections of SPC Mesoscale Analysis: https://www.spc.noaa.gov/exper/mesoanalysis/new/viewsector.php?sector=19.

[2] Hereafter, the effective-layer STP currently in operation will be referred to as the current STP or simply STP. Any references to the fixed-layer versions or modifications to the current STP will be labeled appropriately (i.e., STPfix).

The nontornadic VORTEX2 composite represents high-end, null supercell cases (i.e., intense, nontornadic supercells in environments conventionally considered favorable for tornadoes), which are particularly problematic for operational warnings. In this paper, we seek to in identify environmental characteristics that discriminate between severe supercells that do produce significant tornadoes with those that do not across a much wider dataset.

In a three part numerical modeling study using the Parker (2014) soundings, Coffer and Parker (2017, 2018) and Coffer et al. (2017) showed that the different lower-tropospheric wind profiles in the VORTEX2 composites resulted in distinct configurations of the low-level mesocyclone, where near-surface streamwise horizontal vorticity resulted in a steady low-level mesocyclone and low-level updraft, which were highly favorable for the intensification of near-surface vorticity into a tornado. Near-surface crosswise horizontal vorticity in the nontornadic VORTEX2 composite led to supercells with disorganized low-level mesocyclones which, because of their unsteady nature, hindered the development of tornadic-strength vortices. Coffer and Parker (2018) further showed that systematic variations in near-ground SRH between these two composite profiles directly influenced the likelihood of tornadogenesis in the simulated supercells. Perhaps most pertinent to the present study, Coffer and Parker (2017) showed that the environmental parcels that made up the low-level mesocyclones (~1 km AGL) in both the nontornadic and tornadic supercells *originated exclusively from below 500 m*. The effective inflow layer generally contains parcels that originate much farther aloft (e.g., 1–3 km AGL), but these parcels do not actually contribute to the low-level mesocyclone.

In the present work, we examine the possibility that tornado forecasts (including the popular STP) could be improved by utilizing the SRH in the lowest few hundred meters of the atmosphere, instead of the much deeper layers currently used operationally. The idea of using the shallower layers for SRH integration is not particularly new. When Rasmussen (2003) incorporated the 0–1-km SRH into the energy helicity index (EHI; Hart and Korotky 1991), as opposed to a deeper layer of 0–3 km, he speculated that an even shallower layer might be better if the utilized proximity soundings had sufficient vertical resolution. This conjecture was supported by Markowski et al. (2003), who found that the only statistically significant difference in SRH between significantly tornadic supercells and nontornadic supercells was in the lowest 500 m AGL. Following that, Esterheld and Giuliano (2008) showed that SRH integrated over the 0–500-m layer provided the best discrimination between observed proximity soundings for nontornadic and tornadic supercells in Oklahoma. Additionally, they found that the angle between the 0–500 m AGL bulk shear vector and the 10-m storm-relative inflow vector (referred to as the "critical angle," hereafter CAngle)[3] was most commonly near 90° for the significantly tornadic supercells (indicating purely streamwise horizontal vorticity). Meanwhile for the nontornadic supercells, the CAngle was much more frequently near 110° (indicating partially crosswise horizontal vorticity).

In addition to the near-ground SRH, the present study also investigates whether directly using the components of the horizontal vorticity (streamwise and/or crosswise) would result in clearer distinctions between nontornadic and significantly tornadic supercells. Such a finding could launch a different approach to tornado forecasting that would be partly incompatible with the current formulation of the STP (e.g., as suggested by Nowotarski and Jensen 2013). We discuss these possibilities in the following subsections.

2. Methods

The severe weather event database[4] used in this study is that of Smith et al. (2012) and Thompson et al. (2012), except expanded to include the years 2005–17 for tornadic thunderstorms and 2005–15 for nontornadic thunderstorms (i.e., all available severe weather events in the current SPC convective mode database). All tornado, significant hail (sighail), and significant wind (sigwind) reports were filtered for the largest magnitude report per hour on a 40-km spacing Rapid Update Cycle (RUC) model analysis grid and then assigned to the closest analysis hour. Subsignificant hail/wind events or null cases (i.e., storms without severe weather reports) were not considered due to the difficulty of subjective case identification associated with what would be an overwhelming sample size (Smith et al. 2012). We argue that, fundamentally, discerning the differences between tornadic and significantly severe, nontornadic storms is the most interesting and challenging forecast problem.

Each severe report was assigned a storm mode classification based on archived level II WSR-88D data from NCEI, as discussed in-depth by Smith et al. (2012).

[3] See Fig. 9 in Esterheld and Giuliano (2008) for an example analysis hodograph with the key components of the CAngle.

[4] Compared to *Storm Data*, this dataset has a higher standard of quality control. Careful temporal or spatial adjustments were made to a small portion of the event database to correct report errors (Smith et al. 2012).

TABLE 1. Event counts for all subclassifications by convective mode category.

Mode	All events	Tornado	Weakly tornadic	Significantly tornadic	Nontornadic	Sighail	Sigwind
Total events	20 194	9355	7743	1612	10 839	7051	3788
Discrete RM	7782	3508	2881	627	4274	3296	978
Cluster RM	9609	4295	3580	715	5314	3228	2086
Line RM	2803	1552	1282	270	1251	527	724

In this study, only the right-moving (cyclonic) supercells (RMs) were considered. Nearly 90% of all significant tornadoes occur with RMs (Smith et al. 2012), while 95% of all fatalities and 92% of injuries occur with significant tornadoes. The RMs classification includes three subclassifications: discrete cell, cell in cluster, and cell in line. This resulted in 9355 tornadoes, 3788 sigwind, and 7051 sighail events (Table 1). These 20 194 right-moving supercells were also categorized as being associated with either 1) significantly severe nontornadic[5] (nontor; 10 839 cases), 2) weakly tornadic (E)F0–1 tornadic damage (weak tor; 7743 cases), or 3) significantly tornadic (E)F2–5 tornado damage (sig tor; 1612 cases). Approximately 54% of the dataset is nontornadic (Table 1), and while this is lower than the expected percentage of nontornadic supercells in nature (approximately 85% of supercells are nontornadic; Thompson et al. 2017), the hourly maximum filtering process omits nontornadic supercells that occur in the same hour and grid cell as a tornadic supercell. Using the subjectively defined geographic regions in Fig. 1, the 1-h max event counts are dominated by the Southeast (SE; which includes the Lower Mississippi Valley and South Atlantic) and the plains (southern plains and northern plains). Approximately 73% of the significant tornadoes and 68% of the nontornadic supercells are in those two regions (Fig. 1). A considerable proportion of the tornadoes rated by EF2+ damage are in the SE (44%), more so than any other region; whereas the plains has the majority of the nontornadic events (53%).

Environmental base-state data corresponding to each severe report were obtained from archived vertical profiles from the SPC's mesoscale surface objective analysis (SFCOA; Bothwell et al. 2002), which itself uses the RUC model[6] as the background environment (Benjamin et al. 2004). Profiles were interpolated to isobaric surfaces with 25-hPa vertical resolution (e.g., 1000, 975, 950, 925 hPa, . . .). Use of isobaric data results in a loss of vertical resolution near the ground. On the native hybrid sigma-isentropic coordinate system, the RUC has roughly nine levels in the lowest kilometer (six below 500 m) versus five levels (three below 500 m) in the isobaric grids through the same depth. This has obvious implications for SRH calculations in the near-ground layer. Regardless, as it will be shown later, there is still forecast skill in the wind profile in the lowest 500 m, despite the loss in vertical resolution. Further comparisons between the native vertical coordinate system and the isobaric grid for the VORTEX2 far-inflow soundings from Coffer (2016) are presented in the appendix.

All sounding-derived parameters were recalculated from the archived gridpoint vertical profiles (causing some values to vary slightly from the archived 2D mesoanalysis fields). These independent calculations were performed in order to expand the available parameters beyond what is routinely archived by the SPC. Calculations of thermodynamic variables (i.e., CAPE, LCL, LFC, etc.) include the virtual temperature correction, and all SRH calculations use the Bunkers storm motion. Boxplots showing the distributions for each parameter, in addition to those discussed herein, are available in the online supplemental material. Subjective comparisons were conducted between our independent calculations and a handful of soundings analysis programs [e.g., NSHARP/SHARPpy (Hart and Korotky 1991; Blumberg et al. 2017), CM1 (Bryan et al. 2003), calcsound (Emanuel 1994), plotskew (http://moe.met.fsu.edu/~rhart/plotskew.gs)]. In general, kinematic calculations were nearly identical between the programs, while thermodynamic calculations had more substantial fluctuations. For example, differences of as much as 200–500 J kg^{-1} in CAPE were possible among the five tested programs for soundings with high CAPE values. These differences arise from different methods for lifting a parcel and computing the eventual equivalent potential temperature (once saturated). The method used in this study on average leads to the lowest CAPE values tested. In comparison, NSHARP/SHARPpy, which was used in previous STP studies, had the largest CAPE values. Biases in the thermodynamic calculations should at least be consistent across the 20 194 proximity soundings presented herein and should not

[5] Hereafter, "nontornadic" is understood to refer to significantly severe nontornadic supercells [i.e., storms that produce ≥2-in. (5.04 cm) diameter hail and ≥65-kt (33.4 m s^{-1}) convective wind gusts].

[6] The Rapid Refresh (RAP) model replaced the RUC model at 1200 UTC 1 May 2012.

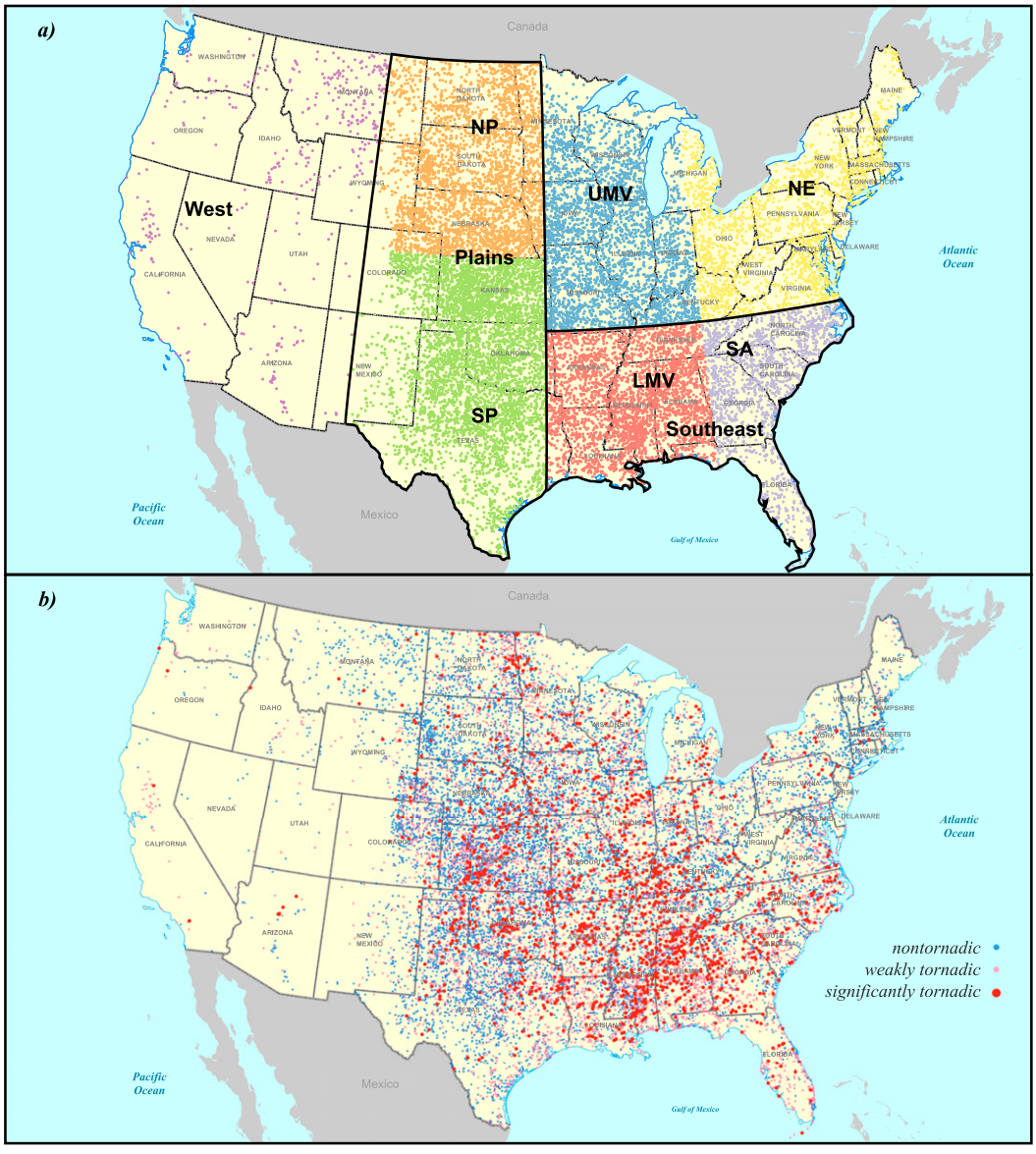

FIG. 1. (a) Map of all right-moving supercell events separated by geographical regions of the United States. Region labels: Northeast (NE), South Atlantic (SA), Lower Mississippi Valley (LMV), Upper Mississippi Valley (UMV), northern plains (NP), southern plains (SP), and western United States (West). Outlined regions delineating the combination of the NP and SP will occasionally be referred to as the plains, while similarly, the combination of the LMV and SA will be referred to as the Southeast. (b) Map of the same events, except separated by significant tornadoes [(E)F2+; red], weak tornadoes [(E)F0–1; pink], and nontornadic severe storms (sighail and sigwind; blue).

impact the main purpose of this paper, which is to explore the forecast utility of near-ground SRH. Implications of the thermodynamic biases and their impact on the magnitude of STP are briefly discussed further in section 4.

As discussed previously, STP is a composite of several useful forecast parameters. The formulation of the effective-layer STP version is

$$\mathrm{STP} = \frac{\mathrm{MLCAPE}}{1500\,\mathrm{J\,kg^{-1}}} \times \frac{2000 - \mathrm{MLLCL}}{1000\,\mathrm{m}} \times \frac{200 + \mathrm{MLCIN}}{150\,\mathrm{J\,kg^{-1}}} \times \frac{\mathrm{EBWD}}{20\,\mathrm{m\,s^{-1}}} \times \frac{\mathrm{ESRH}}{150\,\mathrm{m^2\,s^{-2}}}, \quad (1)$$

where the MLLCL term is set to 1.0 when MLLCL $<$ 1000 m, and set to 0.0 when MLLCL $>$ 2000 m; the MLCIN term is set to 1.0 when MLCIN $> -50\,\mathrm{J\,kg^{-1}}$,

and set to 0.0 when MLCIN $< -200\,\mathrm{J\,kg^{-1}}$; the EBWD term is capped at a value of 1.5 for EBWD $> 30\,\mathrm{m\,s^{-1}}$, and set to 0.0 when EBWD $< 12.5\,\mathrm{m\,s^{-1}}$. Last, the entire index is set to 0.0 when the effective inflow base is above the ground.

A rigorous assessment of each forecast parameter is accomplished using a classic 2×2 contingency table (Doswell et al. 1990; Doswell and Schultz 2006), testing a range of threshold values for each candidate variable. The true skill statistic (TSS, also known as the Pierce skill score; Wilks 2011, chapter 8) is used in order to determine which environmental parameters are most skillful at discriminating between nontornadic and significantly tornadic supercells. The TSS highlights parameters that maximize probability of detection (POD; or "hit rate") while minimizing probability of false detection (POFD; or "false alarm rate"). The TSS is defined by

$$\mathrm{TSS} = (ad - bc)/(a + c)(b + d), \tag{2}$$

where a is the sum of correct forecasts of a significant tornado report, b is the sum of false alarms, c is the sum of missed significant tornado reports, and d is the sum of correct null forecasts. TSS is also equivalent to the difference between the POD and the POFD (Doswell et al. 1990), meaning that parameters with high TSS have an optimal combination of detecting events without misidentifying nulls. Other metrics of forecast skill, including receiver operating characteristics (ROC), the area underneath the ROC curve (AUC), and the Heidke skill score (HSS) were tested. Their trends were generally similar to the TSS.

A TSS value of 1.0 indicates a perfect forecast, while 0.0 is a random forecast of no skill. Since significantly tornadic supercells are, by their nature, rare atmospheric events, the infrequency of even high-end supercells to produce tornadoes can result in relatively poor skill scores (Togstad et al. 2011). The occurrence of supercells, and especially tornadoes, depends on many factors other than the simple overlap of environmental parameters in the STP equation (e.g., the development and evolution of convection, which is still rather poorly forecasted; Hart and Cohen 2016). STP's primary function is to highlight general areas with a favorable combination of ingredients, and here we ask whether those ingredients can be further improved.

3. Characteristics of the near-ground kinematic profile

Recent research has suggested that shallower layers of SRH integration may be more skillful than the deeper layers (e.g., the effective inflow layer) more commonly used in operational settings. Other characteristics of the near-ground kinematic profile, including the streamwise and crosswise components of the horizontal vorticity, are also candidates to provide further skill. In this section, we discuss the forecast skill associated with various ways of characterizing the lower-tropospheric wind profile.

a. Shallower layers of SRH

Using progressively shallower depths for the integration of SRH results in increasing forecast skill when comparing significantly tornadic supercells to nontornadic supercells (Tables 2 and 3). Not surprisingly, SRH in the 0–3 km AGL layer has the lowest utility, with a $\mathrm{TSS_{SRH3}}$ of 0.434. This lower forecast skill is why Rasmussen (2003) refined the EHI parameter to incorporate SRH1 instead of SRH3. The next shallowest layer, on average, is the effective inflow layer, which has a median depth of 2230 m AGL for surface based supercells, which is 500 m deeper than in the Thompson et al. (2007) dataset (there were no differences in the distributions of inflow layer depths between nontornadic and significantly tornadic surface-based supercells). The forecast skill for the ESRH is only marginally better than SRH3 (Table 3). $\mathrm{TSS_{ESRH}}$ is 0.446 at an optimal threshold of approximately $250\,\mathrm{m^2\,s^{-2}}$ (Table 3).

There is a substantial jump in SRH forecast skill when the calculation is focused in the lowest kilometer of the troposphere. Going from the effective inflow layer to the 0–1-km layer, $\mathrm{TSS_{SRH1}}$ increases to 0.508 (Table 3). There are even further increases for shallower layers. SRH in the lowest 500 m AGL has the highest forecast utility of any of the indices tested within the current dataset ($\mathrm{TSS_{SRH500}} = 0.529$).[7] Increases in TSS within shallower layers is predominately driven by decreases in FAR. The median value of SRH500 for significantly tornadic supercells is 3.5 times higher[8] than the median for nontornadic supercells ($224\,\mathrm{m^2\,s^{-2}}$ vs

[7] Even shallower layers of SRH have slightly more skill (i.e., $\mathrm{TSS_{SRH250}} = 0.532$), however due to the isobaric vertical grid, oftentimes this only represents a single, unique vertical level. We chose to focus on the 0–500 m AGL layer herein due to the similar skill scores and more unique data points. It is possible that even shallower layers would have increased skill if higher-resolution environmental profiles were available.

[8] SRH for significantly tornadic supercells could actually be underestimated, as well, because environments with large SRH are observed to produce more off-hodograph deviation in the storm motion. This is a situation that the Bunkers storm motion estimate (which is uniformly used in the SRH calculations) struggles with (Bunkers et al. 2000, 2014; Bunkers 2018).

TABLE 2. Median values for given forecasting parameters across three tornado damage classes of all RMs (discrete cell, cell in cluster, and cell in line). The RM nontor category consists of only significant hail and significant wind events, with no tornado reports within ±3 h and 185 km.

	RM EF2+	RM EF0–1	RM nontor	RM EF2+−RM EF0–1 (% change)	RM EF2−RM EF nontor (% change)
MLCAPE (J kg^{-1})	995.41	883.40	1148.27	13	−13
MLCIN (J kg^{-1})	−10.72	−8.93	−19.21	20	−44
MLLCL (m AGL)	800.0	850.0	1080.0	−6	−26
EBWD (m s^{-1})	27.59	22.68	22.56	22	22
SRH500 (m^2 s^{-2})	224.04	126.81	63.69	77	252
SRH1 (m^2 s^{-2})	317.06	190.06	108.39	67	193
SRH3 (m^2 s^{-2})	393.29	265.84	204.31	48	93
ESRH (m^2 s^{-2})	360.5	230.01	167.25	57	116
SW500 (s^{-1})	2.46×10^{-2}	1.68×10^{-2}	8.86×10^{-3}	46	177
CW500 (s^{-1})	5.45×10^{-3}	5.11×10^{-3}	4.92×10^{-3}	6	10
ratio500	3.76	2.54	1.17	48	222
diff500 (s^{-1})	1.67×10^{-2}	8.32×10^{-3}	8.98×10^{-4}	101	1765
CAngle (°)	63.48	70.94	78.39	—	—
SCP	10.40	5.73	4.86	82	114
STP	1.65	0.64	0.37	158	352
STPfix	1.77	0.84	0.41	112	331
STP500	1.75	0.62	0.19	181	812
3CAPE (J kg^{-1})	54.39	53.72	40.94	1	33
LR3 (°C km^{-1})	5.998	6.136	6.546	−2	−9
VTP	1.36	0.50	0.23	171	494
SHERB	1.20	0.95	0.94	25	27
VGP	0.24	0.19	0.18	26	32

64 m^2 s^{-2}, respectively; Fig. 2; Table 2). Filtering the dataset to only include surface-based storms (i.e., the effective inflow base is at the ground), further increases the skill of SRH500 ($TSS_{SRH500} = 0.563$). While outliers are not shown in Fig. 2 for clarity, there are also many more cases with negative SRH in the lowest 500 m AGL in the nontornadic subset of supercells, even though the overall wind profile supports right-movers. For nontornadic supercells, 12.2% of the dataset has SRH500 values below 0 m^2 s^{-2}. In contrast, only 0.86% of the significantly tornadic subset of supercells has negative SRH500.

As might be expected, there is regional variance in the forecast skill of SRH500. Using the defined regions in Fig. 1, the forecast utility of SRH500 is highest in the Southeast and the Northeast regions of the United States (Table 4). In particular, the South Atlantic region has a TSS_{SRH500} of 0.588 (Table 4), a substantial increase compared to the national average. In comparison, both the northern and southern plains have a TSS_{SRH500} that is quite a bit lower than the national average ($TSS_{SRH500} = 0.406$; Table 4). Skill of SRH500 in the western United States is even lower, although the sample size of significant tornadoes there is particularly small ($n = 10$). We comment on the regional variability in skill further in section 4.

The forecast skill for SRH500 is highest for discrete cell RMs and then cell in cluster RMs, while the skill in SRH500 for RMs in lines is appreciably worse (not shown). The median value of SRH500 for line RMs is considerably higher than the other two subclasses of RMs (especially for nontornadic supercells), possibly because line RMs occur most frequently in the Southeast (Smith et al. 2012, see their Fig. 7) where SRH500 is typically higher. The reason for lower skill in line RMs could be indicative of physical differences between the storm types, such as the pathway(s) for tornadogenesis failure is more easily obtainable for line RMs than their more isolated counterparts (e.g., increased cell interactions and more negatively buoyant surface outflow), despite occurring in seemingly favorable environments. Additionally, even more lower-tropospheric SRH is perhaps required for line RMs to establish a steady, intense low-level mesocyclone capable of producing a significant tornado.

In summary, progressively shallower layers for the SRH calculation leads to increasing forecast skill, particularly for the more discrete RM supercell cases. Next, we consider whether the tornado forecasting process could be improved by looking at not only the streamwise component of the horizontal vorticity but also the the crosswise component.

b. *Individual components of streamwise/crosswise horizontal vorticity*

One of the working hypotheses at the outset of this study was that nontornadic supercells would have

TABLE 3. Best TSS and optimal threshold for given forecasting parameters for discriminating between significant tornadoes (EF2+) and significant hail/wind events. TSS is calculated at 100 evenly spaced numbers between the 5th and 95th percentile of the entire RUC/RAP sounding dataset for each variable. Units are given in Table 2.

	Max TSS	Optimal threshold
MLCAPE	0.025	2886.31
MLCIN	−0.133	−25.22
MLLCL	−0.294	909.10
EBWD	0.317	25.83
SRH500	0.529	144.3
SRH1	0.508	189.0
SRH3	0.434	280.69
ESRH	0.446	252.73
SW500	0.527	1.73×10^{-3}
CW500	0.042	3.39×10^{-3}
ratio500	0.355	1.88
diff500	0.489	1.02×10^{-2}
SCP	0.304	6.30
STP	0.364	0.86
STPfix	0.425	0.89
STP500	0.451	0.83
3CAPE	0.094	31.03
LR3	0.068	4.75
VTP	0.271	1.82
SHERB	0.302	0.98
VGP	0.234	0.22

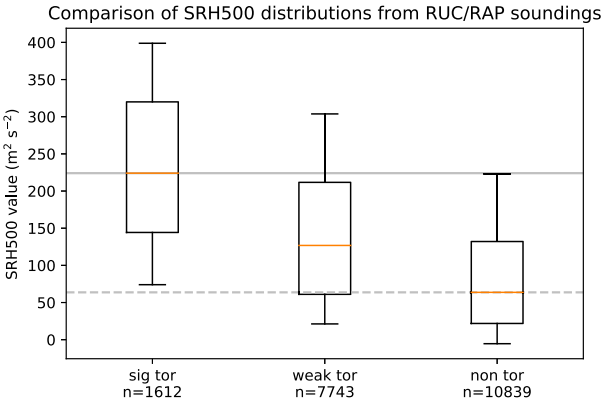

FIG. 2. Box-and-whisker plot of 0–500 m AGL SRH (SRH500; $m^2 s^{-2}$) for all RMs by significant tornadoes [(E)F2+], weak tornadoes [(E)F0–1], and nontornadic severe storms (sighail and sigwind) for all RMs. The solid gray line represents the median of sig tor SRH500, and the dashed gray line represents the median of the nontor SRH500. The boxes span the 25th–75th percentiles, and the whiskers extend upward to the 90th and downward to the 10th percentiles. Outliers are excluded for clarity. Sample sizes *n* for each damage class are shown for reference.

higher values of crosswise horizontal vorticity than their significantly tornadic counterparts. Historically, only the streamwise component of the horizontal vorticity has been considered in the forecast process (particularly, its integrated flux in the form of SRH). However, storms ingest air consisting of both streamwise and crosswise horizontal vorticity and the pair of components influence the storm structure and thus the eventual probability of tornadogenesis (e.g., Davies-Jones 1984; Coffer and Parker 2017). A few observational studies have noted the presence of predominately crosswise vorticity in the lowest few hundred meters in a subset of nontornadic supercells (Markowski et al. 2003; Esterheld and Giuliano 2008; Nowotarski and Jensen 2013; Parker 2014). It is possible that looking at both the streamwise and crosswise components of horizontal vorticity in tandem could lead to clearer boundaries between environments of nontornadic and significantly tornadic supercells than SRH alone. After all, high SRH is commonly achievable when the lower-tropospheric environmental vertical wind shear vector magnitude is large, even if the orientation of near-surface horizontal vorticity is predominately crosswise (i.e., the nontornadic VORTEX2 composite profile).

Unsurprisingly, the streamwise component of the horizontal vorticity in the lowest 500 m AGL displays almost identical skill to SRH in discriminating between nontornadic and significantly tornadic supercells (Table 3). For the crosswise component of the horizontal vorticity, we tested the magnitude of crosswise vorticity, under the presumption that any amount of crosswise vorticity, whether it be positive or negative, is detrimental to the low-level organization of the storm (Coffer and Parker 2017). Contrary to our initial hypothesis, the three sets of supercells display inconsequential differences in the median value of crosswise vorticity in the lowest 500 m AGL (Table 2), as well as through other depths (not shown). Independent calculations of crosswise horizontal vorticity using the Bunkers et al. (2014) proximity sounding dataset results in similar conclusions (M. Bunkers 2019, personal communication).

Coffer and Parker (2018) also speculated that the ratio of streamwise to crosswise vorticity could serve as a forecasting parameter, as their simulated supercells became progressively more likely to produce tornadoes when there was much more streamwise than crosswise horizontal vorticity in the 0–500 m AGL layer. Herein, we examine this ratio as well as the difference between the two horizontal vorticity components, as the streamwise/crosswise ratio is problematic for 2 reasons: 1) the ratio will approach infinity as crosswise vorticity approaches zero, and therefore 2) the ratio can be large even if the streamwise horizontal vorticity is negligible. Neither of these parameters, the streamwise/crosswise vorticity ratio nor the streamwise/crosswise vorticity difference, have as much forecast skill as SRH

TABLE 4. As in Table 3, but for the subjectively defined regions shown in Fig. 1.

	NE		SA		LMV		UMV		NP		SP		West	
	Max TSS	Optimal threshold	Max TSS	Optimal threshold	Max TSS	Optimal threshold	Max TSS	Optimal threshold	Max TSS	Optimal threshold	Max TSS	Optimal threshold	Max TSS	Optimal threshold
MLCAPE	−0.048	2202.66	−0.01	22.75	0.055	100.46	0.102	262.35	0.238	1856.01	0.211	1919.2	0.083	194.06
MLCIN	−0.089	0.0	0.126	1.805	0.078	0.0	0.106	42.29	0.258	55.64	0.134	26.77	0.389	7.58
MLLCL	0.181	846.97	0.34	748.71	0.25	803.76	0.257	899.09	0.221	1191.71	0.24	1090.1	0.484	1167.12
EBWD	0.398	23.5	0.422	24.75	0.276	26.26	0.378	25.69	0.132	26.76	0.212	25.86	0.159	20.29
SRH500	0.582	132.75	0.588	129.18	0.471	171.07	0.496	168.45	0.408	66.15	0.405	150.78	0.389	21.58
ESRH	0.466	185.68	0.489	238.11	0.461	295.18	0.51	255.91	0.294	229.51	0.35	254.07	0.167	76.10
SCP	0.345	3.91	0.320	5.06	0.299	7.95	0.348	7.49	0.373	10.19	0.378	8.50	0.119	1.78
STP	0.250	0.773	0.327	0.942	0.283	1.3	0.380	0.767	0.420	1.350	0.426	0.862	0.298	0.126
STPfix	0.362	0.543	0.406	1.024	0.335	0.951	0.426	1.265	0.493	1.121	0.472	0.931	0.294	0.149
STP500	0.291	0.657	0.409	0.639	0.318	1.123	0.456	0.856	0.496	0.877	0.475	0.806	0.361	0.042
3CAPE	−0.009	0.309	−0.031	0.064	0.036	0.012	0.126	23.98	0.288	38.69	0.185	43.73	0.278	53.451
LR3	−0.028	5.15	−0.007	4.789	0.049	4.861	0.198	5.330	0.128	5.029	0.071	5.462	0.143	6.337

alone (Tables 2 and 3). This is due to the lack of forecast skill in the crosswise horizontal vorticity. In short, there appears to be no need for a paradigm shift in what forecasters use since SRH has the highest forecast skill among closely related parameters.

c. *Critical angle*

The CAngle, first introduced by Esterheld and Giuliano (2008), is a proxy for how streamwise the horizontal vorticity is at 10 m AGL. The angle is computed between the 0–500 m AGL shear vector and the 10-m storm-relative inflow vector. Esterheld and Giuliano (2008) found that for a sample of 67 cases in Oklahoma, the CAngle was most commonly near 90° for the significantly tornadic supercells (indicating purely streamwise horizontal vorticity). Meanwhile for the nontornadic supercells, the CAngle was much more frequently near 110° (indicating partially crosswise horizontal vorticity).

Contrary to their findings, the median CAngle within the present database is near 65° for significantly tornadic supercells (Table 2). The median CAngle for nontornadic storms is actually closer to purely streamwise (~80°). However, density histograms of the two populations show that the peak of both distributions is nearly the same (~60°), although the nontornadic distribution has much wider tails (Fig. 3). Therefore, CAngle seems to mostly matter if it is very large (>120°) or small (<30°), which in both cases would typically be associated with nontornadic supercells.

Hodographs with CAngle values near 90° might not be as common in the atmosphere within a large diverse dataset such as this compared to Esterheld and Giuliano (2008), although this finding could be impacted by the RUC's representation of the planetary boundary layer (PBL; more on this in the appendix). Another potential difference between this study and Esterheld and Giuliano (2008) is their use of observed storm motions compared to forecasted forecasted motions used herein. CAngle is a highly volatile parameter that is sensitive to minor changes in the storm motion, surface wind direction, and lower-tropospheric wind profile (M. Bunkers 2019, personal communication). CAngle might work best when the shape of the hodograph loosely resembles the canonical "Weisman–Klemp" quarter-circle, as it was developed using cases solely from Oklahoma. In any case, even when the CAngle is far from 90°, the SRH in the near-surface layer may still be quite large. This reflects a limitation of using only two vectors to estimate streamwise vorticity at a single height in the CAngle calculation. Since SRH is integrated over a layer and is directly related to the

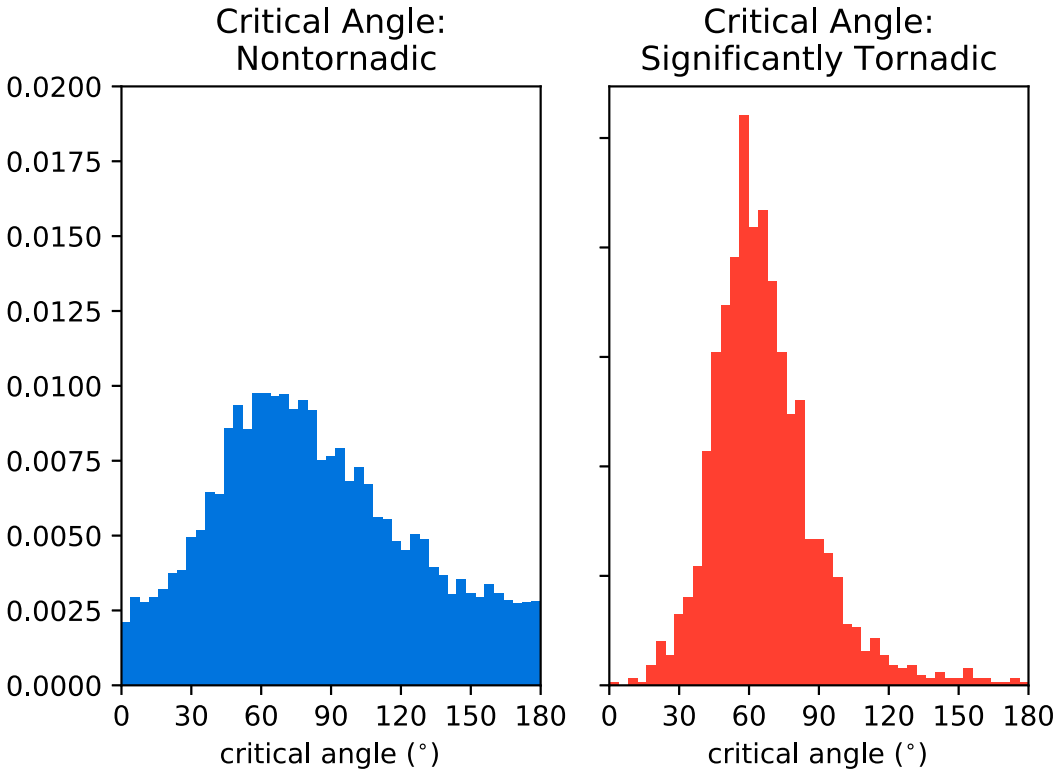

FIG. 3. Density histogram plot of critical angle (°) for (left) nontornadic severe storms (sighail and sigwind) and (right) significant tornadoes [(E)F2+] for all RMs. The counts are normalized to form a probability density [i.e., the area (or integral) under the histogram sums to 1]. This is achieved by dividing the count by the number of observations times the bin width.

circulation of the mesocyclone, it is more robust (and produces more skill) than CAngle.

4. Improvements to the STP with SRH500

A motivating factor for this work was to determine whether the most commonly used forecasting parameter for significantly tornadic supercells could be improved by using the near-ground storm relative helicity. According to the SPC website: "Of the three SRH calculations displayed on the SPC mesoanalysis page, effective SRH is the most applicable across the widest range of storm environments, and effective SRH discriminates as well as 0–1-km SRH between significant tornadic and nontornadic supercells." However, in section 3a, it was shown that, at least for right-moving supercells, progressively shallower layers of SRH display greater discrimination between nontornadic and significantly tornadic supercells. In this section, we will compare the current STP with a variant that uses SRH500 instead of ESRH. Following that, we will discuss the relative contributions of the five ingredients to the overall forecast skill of STP and STP500.

a. *Effective-layer STP versus STP with 0–500 m AGL SRH*

The combination of parameters in Eq. (1) results in the well-known skill of the effective-layer STP. The median STP for significant tornadoes is 1.65, while the

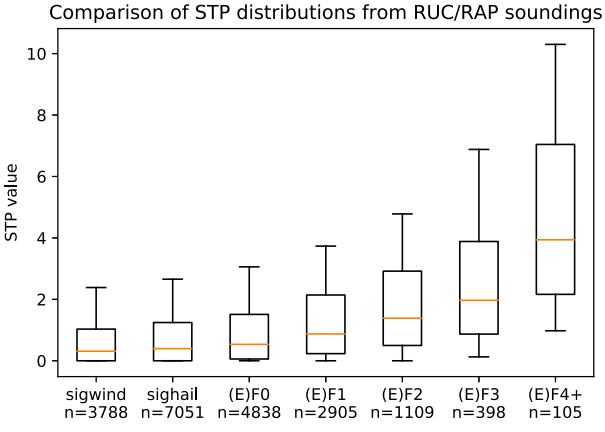

FIG. 4. Box-and-whisker plot of effective-layer STP (dimensionless) for all RMs by (E)F-scale damage rating classes, including nontornadic RMs that produced only significant wind or significant hail. Other plotting conventions are as in Fig. 2.

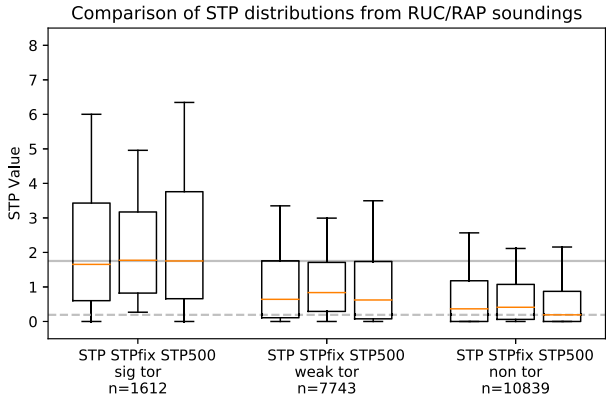

FIG. 5. Box-and-whisker plot of effective-layer STP, fixed-layer STP, and STP500 (dimensionless) for all RMs by significant tornadoes [(E)F2+], weak tornadoes [(E)F0–1], and nontornadic severe storms (sighail and sigwind). The solid gray line represents the median of sig tor STP500, and the dashed gray line represents the median of the nontor STP500. Other plotting conventions are as in Fig. 2.

median STP for nontornadic supercells is 0.37 (Table 2). In discriminating between significantly tornadic and severe nontornadic supercells, the overall forecast skill of the STP is 0.364, an improvement compared to the SCP (Table 3). As in previous studies, there is a noticeable increase in effective-layer STP with increasing (E)F-scale damage rating for all damage classes and at all percentile ranks [Fig. 4, cf. Fig. 12 in Thompson et al. (2012)]. Increases in the median and percentile ranks are proportionally similar to Thompson et al. (2012), despite the independent calculation of parameters performed herein. From Fig. 4 and comparisons to Thompson et al. (2012), we are confident that any potential biases in our recalculated thermodynamic parameters (described in section 2) were at least consistent across all cases.

In the present work, a slight modification to the STP is proposed, where ESRH is replaced with the 0–500-m SRH (SRH500):

$$\text{STP500} = \frac{\text{MLCAPE}}{1500\,\text{J kg}^{-1}} \times \frac{2000 - \text{MLLCL}}{1000\,\text{m}} \times \frac{200 + \text{MLCIN}}{150\,\text{J kg}^{-1}} \times \frac{\text{EBWD}}{20\,\text{m s}^{-1}} \times \frac{\text{SRH500}}{75\,\text{m}^2\,\text{s}^{-2}}, \quad (3)$$

each parameter is capped at the same values as the STP. Additionally, the 0–500-m layer used for SRH integration is required to be within the effective inflow layer (or else the parameter is set to 0.0), in order to continue the practice of omitting cases that are not likely to be surface based. The normalization denominator of $75\,\text{m}^2\,\text{s}^{-2}$ for SRH500 in Eq. (3) was subjectively chosen to obtain a similar distribution[9] of STP500 compared to STP for significantly tornadic supercells (i.e., preserving the common threshold of 1 used to discriminate between significant tornadoes and nontornadic supercells).

TABLE 5. Number of hits and correct nulls (second column) and misses and false alarms (third column), identified when utilizing the given composite parameters at their optimal thresholds shown in Table 3.

	Correct	Incorrect
SCP	7594	4857
STP	8467	3984
STPfix	8805	3646
STP500	9172	3279

Since shallower layers of SRH have even more forecast skill than SRH integrated through the effective inflow layer, it is no surprise that, when using Eq. (3), the TSS of STP500 increases to 0.451 (Table 3). The improvements in STP500 compared to STP and STPfix are mainly due to a shift in the distribution of nontornadic supercells toward values of zero (Fig. 5). The median in STP500 for significantly tornadic supercells is approximately equal to the 87th percentile of nontornadic supercells (Fig. 5). While the improvements offered by STP500 may appear modest in the box-and-whisker plots, the change results in an 8% increase in number of correctly predicted events and an 18% decrease in missed events and false alarms compared to the current STP at their respective optimal thresholds (Table 5).

There is substantial spatial variance in the forecast utility of STP500 across the United States. $\text{TSS}_{\text{STP500}}$ is highest in the plains, specifically the northern plains ($\text{TSS}_{\text{STP500}} = 0.496$; Table 4). Forecast skill in the Upper Mississippi Valley is also higher than the national average ($\text{TSS}_{\text{STP500}} = 0.456$; Table 4). The TSS values are quite a bit lower in the SE United States, where the $\text{TSS}_{\text{STP500}}$ decreases to 0.355 (Table 4). The lower skill in the SE United States is due to the loss in forecast skill for both MLCIN and MLCAPE (discussed in more detail in the following subsection). MLCIN has essentially no skill in the SE, while MLCAPE actually has substantial negative skill throughout most of the distribution (i.e., CAPE is on average higher for nontornadic storms). The decrease in $\text{TSS}_{\text{STP500}}$ is in spite of the increase in forecast skill for SRH500 and EBWD in the SE (Table 4). Forecast skill for STP500 is even worse in

[9] The choice of this value does not affect the overall forecast skill of the parameter, as it simply shifts the distribution uniformly up (down) and leads to higher (lower) optimal thresholds between significantly tornadic supercells and nontornadic supercells.

the western and northeastern United States (Table 4); however the sample size for significant tornadoes in these regions is extremely small. Despite these regional variances, *in every region STP500 outperforms the current effective-layer STP* (as measured by the TSS; Table 4).[10]

b. *Forecast skill of individual components of STP*

The individual components of STP have varying degrees of utility. The median in MLCAPE is actually higher in severe nontornadic supercells than the significantly tornadic events (Table 2). The percent change in median MLCAPE between nontornadic supercells and both weakly tornadic and significantly tornadic supercells is fairly negligible (±13%; Table 2). For comparison, the median of MLCAPE in Thompson et al. (2012) is 4% higher in significantly tornadic discrete right movers than severe nontornadic supercells. In either case, this results in the STP having almost no added skill from MLCAPE within the current nationwide dataset, and any positive skill exists only for extreme values of CAPE (Table 3). On the regional scale, MLCAPE has substantial negative skill through the majority of the distribution in the Northeast, Lower Mississippi Valley, and the South Atlantic (up until approximately 1500 J kg^{-1}; Table 4). Meaningful positive skill in CAPE is present for the Upper Mississippi Valley as well as the northern and southern plains (Table 4).

CAPE, on its own, has not shown a consistent ability to discriminate between nontornadic and tornadic supercells in varying environments (Rasmussen and Blanchard 1998; Monteverdi et al. 2003; Sherburn and Parker 2014). Furthermore, tornado warning hits and misses occur in overlapping MLCAPE values (Anderson-Frey et al. 2016). Despite these issues, in the relatively rare cases where large MLCAPE overlaps with high lower-tropospheric SRH and low LCL heights, violent tornadoes are much more common (Fig. 4), even in the SE where MLCAPE has no skill across the entire dataset (i.e., 27 April 2011; Knupp et al. 2014). The lack of overall skill in MLCAPE within the current dataset is at least partly because the nontornadic supercells identified for this study all produced significant hail or significant wind reports. This dataset does not represent a comprehensive nontornadic thunderstorm sample since it does not include subsevere supercells or QLCSs. Despite the minimal (or even negative) skill in MLCAPE, its inclusion in the STP is beneficial in discriminating between thunderstorm environments and environments that do not support deep convection. This reduces the overall FAR area of the STP compared to using solely kinematic components (e.g., shear terms like SRH500 are ubiquitously high in the winter months and to the north of the surface warm sector).

CAPE's best discriminatory value may be between violent tornadoes [(E)F4+] and weakly or nontornadic supercells (Smith et al. 2015; Hampshire et al. 2018). In this dataset, the vast majority of the significantly tornadic supercell events are EF2s, which have a similar MLCAPE distribution to EF0–1 tornadoes [see Fig. 9 in Smith et al. (2015)]. The median MLCAPE value for violent tornadoes (EF4+) is almost 80% higher than EF2 tornadic supercell events. The increases in MLCAPE with increasing EF-scale rating suggests its inclusion in the STP formulation is therefore supported for at least some of its operational applications. Future studies could examine alternative ways to handle MLCAPE in a forecasting parameter such as the STP.

In comparison to MLCAPE, both MLCIN and MLLCL height provide better discrimination between nontornadic supercells and significantly tornadic supercells, with TSS values of −0.13 and −0.29, respectively (Table 3). Values of TSS for these parameters are negative because they have a negative influence on probability of tornadogenesis (e.g., Markowski et al. 2003; Davies 2004) and thus are treated as a penalty in the STP equation [Eqs. (1) and (3)]. MLCIN displays similar regional variations as MLCAPE, having zero (or even negative) skill through much of the eastern United States (Table 4). On the other hand, MLLCL in each region has fairly good forecast skill (Table 4) and is perhaps the most consistent parameter tested herein, with respect to region-by-region forecast skill.

Kinematic components of the STP have a higher forecast skill overall than the thermodynamic parameters. Supercells become more probable as the EBWD increases in magnitude through the range of 12.5–20 m s^{-1} (Thompson et al. 2007). For severe supercells of all types, the EBWD is most often greater than 20 m s^{-1} (Table 2). The maximum TSS_{EBWD} in discriminating between significantly tornadic and nontornadic supercells is 0.317 at an optimal threshold of just over 25 m s^{-1} (Table 3). EBWD is most useful in the Northeast, Upper/Lower Mississippi Valley, and especially the South Atlantic regions (Table 4). Forecast skill for EBWD is much lower in the northern plains and the western United States (Table 4).

The key driver in forecast skill for the current STP is the ESRH; it has by far the greatest TSS among

[10] In every region except the western United States, STPfix is also more skillful than the effective-layer STP, and in some regions it is comparable to the STP500. The latter result likely indicates that in some regions, the surface-based parcel used in the STPfix provides more skill than the mixed-layer parcel and/or the 6BWD versus the EBWD.

the components of STP. The median value for significantly tornadic supercells is 116% higher than for nontornadic supercells (Table 2), yielding a TSS_{ESRH} of 0.446 at an optimal threshold of approximately $250\,m^2\,s^{-2}$ (Table 3). Notwithstanding the skill that ESRH adds to the STP, as documented above in section 4a, the SRH500 is even more useful. In fact, SRH500 alone is more skillful than any STP variant (including STP500) because it does not suffer from the low/negative skill associated with CAPE (although one cannot forecast the general development of tornadic thunderstorms using SRH500 alone). Across the regions, both ESRH and SRH500 remain the most skillful of the STP ingredients but contribute most in the NE, SA, UMV, and LMV and contribute least in the plains and the western United States (Table 4).

Additional forecast verification metrics, including POD, success ratio (1 − FAR), bias *B*, and critical success index (CSI) for each of the components in the STP500 are shown Fig. 6. As discussed in Roebber (2009), for good forecasts, POD, SR, *B*, and CSI approach unity, such that a perfect forecast lies in the upper right of the diagram and optimal increases in accuracy are obtained by moving toward the upper right at a 45° angle. Not surprisingly, MLCAPE is the main outlier in terms of forecast skill relative to the other components of the STP. Not only does it display a low probability of detection, but events are often underforecasted (i.e., biased low), a product of the maximum value of TSS being optimized at extreme MLCAPE values (Table 3). The next three most useful components, MLLCL, MLCIN, and EBWD, are clustered together with CSI values near 0.45. MLCIN is slightly overforecasted at its optimal threshold of $-50\,J\,kg^{-1}$, but none of the three are substantially biased. Finally, for these proximity soundings, SRH500 is the best discriminator between nontornadic and significantly tornadic storms. At a threshold of $150\,m^2\,s^{-2}$, SRH500 has a high POD and low FAR, with a CSI value greater than 0.6 and almost no bias.

In summary, thermodynamic components of STP and STP500 had generally less skill than their kinematic counterparts. Within the dataset of severe supercells tested here, MLCAPE provides no skill to the STP parameter, while MLCIN has a positive, albeit marginal contribution (both are highly regionally dependent as well). MLLCL and EBWD are fairly skillful, while the ESRH and (even more so) SRH500 components by far discriminate the best between nontornadic and significantly tornadic supercells. Of course, as with all model-based proximity soundings, these findings reflect the RUC/RAP's estimation of the environment. We discuss in more detail the mesoanalysis representation of lower-tropospheric kinematic fields in the appendix.

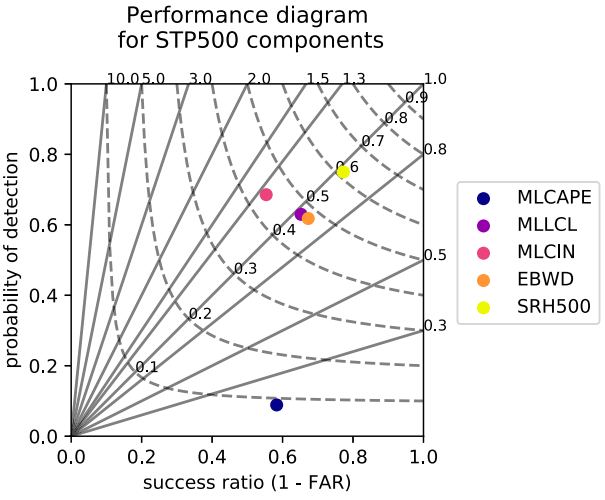

FIG. 6. Performance diagram (Roebber 2009) summarizing the success ratio [1 − FAR (false alarm ratio)], probability of detection, bias, and critical success index at the optimal true skill score for each component of the STP500, which includes mixed-layer CAPE (MLCAPE), mixed-layer LCL (MLLCL), mixed-layer CIN (MLCIN), effective-layer shear (EBWD), and 0–500 m AGL SRH (SRH500). Solid lines represent bias scores with labels on the outward extension of the line, while labeled dashed contours are CSI.

5. Discussion

In recent years, other variants of forecast parameters have been proposed. Some of these involve measures of low-level instability, including the 0–3-km CAPE (3CAPE) and 0–3-km lapse rates (3LR). Examples of this include the enhanced stretching potential (ESP; Caruso and Davies 2005), the severe hazards in environments with reduced buoyancy (SHERB; Sherburn and Parker 2014), and the violent tornado parameter (VTP; Hampshire et al. 2018). While none of these were specifically designed to work across all environments and forecast scenarios, the SCP and the STP are more skillful at discriminating between significantly tornadic and nontornadic supercells than any of the three (Table 3). The VTP does have considerable skill in its intended purpose of discriminating violent tornadoes [(E)F4+] from significant tornadoes (max $TSS_{VTP} = 0.335$, optimal threshold = 7.96), although this is slightly lower than the STP's skill for the same purpose.

The reasoning for the lack of skill in these parameters is twofold: 1) 0–3-km CAPE has relatively low forecast skill (Table 3), although the skill is substantially higher than MLCAPE,[11] and 2) counterintuitively, and perhaps nonphysically, nontornadic supercells on

[11] Using 3CAPE instead of MLCAPE in the STP does not result in a net improvement in forecast skill because soundings with high 3CAPE are not necessarily the same soundings with high SRH500.

average have higher 0–3-km lapse rates than significantly tornadic storms (Table 2). There is actually considerable forecast skill in considering the 0–3-km lapse rate as a negative influence on the tornadogenesis process ($TSS_{LR3} = -0.25$), more so than any other component of the thermodynamic profile besides MLLCL (Table 3). Low-level lapse rates are moderately, inversely correlated with SRH500 ($r^2 \approx 0.5$) and strongly, inversely correlated with MLLCLs ($r^2 \approx 0.7$) due to deep, well-mixed boundary layers having weaker vertical shear profiles and lower relative humidity in the PBL. This indicates that these nontornadic supercell scenarios have other known problems, which may be related to how the dataset is constructed (i.e., majority of severe, nontornadic supercells occur in the Plains; Fig. 1b). This peculiarity with low-level lapse rates may also further speak to issues with the physical parameterization of surface fluxes within the PBL, as discussed in the appendix. Hampshire et al. (2018) showed NWS rawinsonde observations had values of low-level lapse rates 0.75° and 0.63°C km^{-1} higher for violent and significant torndaoes, respectively, compared to the SFCOA. It is possible that PBL schemes struggle in environments with large lower-tropospheric shear combined with steep lapse rates, a condition that violates various similarity theories used for turbulence closures (Stull 1988).

A renewed study of a wide range of parameters utilizing novel data sources, such as the High Resolution Rapid Refresh (HRRR; Benjamin et al. 2016), may lead to better model depictions of differences between environments of nontornadic and significantly tornadic supercells. Not only would the HRRR improve upon the spatial resolution of previous studies, but its advanced data assimilation techniques could improve accuracy in the problematic PBL. Unfortunately, higher-resolution model data also come with trade offs. In trying to create an independent proximity sounding database using the HRRR, Coffer et al. (2018) found it difficult to systematically isolate soundings that were convectively contaminated or influenced by the nearby storms on the convection-allowing grid (even within the 0-h analysis). In the present work, vertical profiles in the SPC's RUC/RAP SFCOA dataset were excluded if the convection parameterization scheme was activated at that grid point.

Given that the lowest few hundred meters of the atmosphere are critically important for so many types of sensible weather, including supercells and tornadoes, our lack of observations in the PBL is a particular obstacle. New technologies, such as unmanned aerial vehicles (UAVs), could better sample the vertical wind profile in the lowest 500 m, with much improved spatiotemporal resolution compared to the current National Weather Service's rawinsonde network and the now defunct wind 404-MHz profiler network (whose minimum height gate was 500 m AGL). Further field projects specifically targeting the inflow region of severe nontornadic and tornadic storms of various convective modes (e.g., as described by Wade et al. 2018) would further help to bridge the gap between the sensitivities revealed by conventional observations, gridded analyses, and high-resolution simulation studies.

6. Conclusions

Recent studies have suggested that the characteristics of the near-ground wind profile may better discriminate between significantly tornadic supercells and nontornadic supercells than the deeper layers currently used in operational forecasting. Proximity soundings derived from the SPC's RUC/RAP SFCOA for 20 194 right-moving supercells show the following key results:

- ESRH has by far the greatest forecast skill for significant tornadoes among the current STP components.
- Using progressively shallower layers of the wind profile for the integration of SRH results in increasing forecast skill. SRH500 is more effective at discriminating between significantly tornadic supercells and nontornadic supercells than ESRH.
- Including SRH500 in the formulation of the STP, instead of ESRH, results in an overall improvement in forecast skill compared to the current STP. The improvements in STP500 are mainly due to a shift in the distribution of nontornadic supercells toward values of zero. STP500 increases the number of correctly predicted events by 8% and decreases missed events and false alarms by 18%.
- There is no statistical difference in the lower-tropospheric crosswise horizontal vorticity between nontornadic, weakly tornadic, and significantly tornadic supercells. Therefore, using a ratio or difference between streamwise and crosswise horizontal vorticity does not result in any additional forecast skill that cannot already be gained from SRH500 alone.

In addition to the primary results above, the following are interesting, ancillary results:

- The critical angle in the RUC/RAP analyses is most commonly near 60° for both nontornadic and significantly tornadic supercells. However, very large CAs (>120°) or small CAs (<30°) heavily favor nontornadic supercells.

- Skill scores of individual forecasting parameters vary widely from region to region. In some regions, a ''one-size-fits-all'' parameter may not be applicable and/or the optimal value is below the common contouring threshold on the operational SPC mesoanalysis.
- Within this dataset, MLCAPE, on its own, has no forecast skill in distinguishing between severe nontornadic, weakly tornadic, and significantly tornadic supercells. MLCAPE's best discriminatory value may be between violent tornadoes and weakly tornadic supercells.

Overall, SRH500 is revealed as a highly skillful parameter for tornado forecasting, and its use would represent a positive modification to the STP. The proposed formulation continues to use the EBWD and require SRH500 to fall within the effective inflow layer, thus retaining the original STP's ability to mask areas where surface-based supercells are unlikely. Interestingly, while STP clearly helps forecasters identify the general area of tornadic thunderstorms (via its inclusion of CAPE, for example), once convection has been deemed likely, additional skill in forecasting significant tornadoes could then be gained by looking more specifically at areas of maximized SRH500. After all, significant tornadoes tend to not occur at the STP maximum but instead along spatial gradients in STP (Cohen 2010; Anderson-Frey et al. 2017). This is likely because SRH is baroclinically maximized near boundaries (Markowski et al. 1998a), and CAPE tends to increase away from surface boundaries (such as warm fronts, drylines, and outflow boundaries). Forecasters still need to maintain operational awareness and not rely solely on parameters (Doswell and Schultz 2006), including looking for positive supercell interactions with surface boundaries or possible failure modes of tornadogenesis (such as destructive storm-to-storm interference and/or upscale growth). Nevertheless, the results of this study provide promising evidence that forecast parameters can still be improved through increased understanding of the environmental controls on the physical processes that govern tornado formation.

Acknowledgments. This research was supported by NSF Grant AGS-1748715. The authors thank John Hart of the SPC for his work on the underlying software used to generate the RUC/RAP proximity sounding database and for the support of SPC management and the SPC Science Support Branch in facilitating operationally relevant projects. We also thank the three anonymous reviewers, as well as the editor Matthew Bunkers, who provided invaluable feedback on this article.

APPENDIX

Kinematic Comparisons between VORTEX2 Soundings and the RUC

The viability of using SPC's RUC/RAP SFCOA data to generate proximity soundings for severe weather events depends on the ability of the analysis to faithfully represent the observed environment. The primary advantage of the RUC/RAP data is their superior spatial and temporal availability. However, model representation of forecast parameters can depend significantly on the assimilation technique and the physical parameterization of surface fluxes within the PBL (e.g., Coniglio et al. 2013; Clark et al. 2015; Cohen et al. 2015). Thus, it is important to validate these models given the wide use of objective analysis systems (such as SFCOA) to diagnose the mesoscale environment (Coniglio 2012). Comparing observed, preconvective soundings from VORTEX2 to RUC soundings, Coniglio (2012) found that biases existed especially in the lower-tropospheric wind profile, where the RUC analyses showed a tendency for the wind speeds to be too fast in the lowest 1 km AGL and too slow in the 2–4 km AGL layer.

The VORTEX2 inflow composite soundings from Parker (2014) contained key, subtle differences between the environments of nontornadic and tornadic supercells. A natural question to ask is whether our best available mesoscale objective analysis (i.e., the RUC in 2009–10) can represent these differences in the wind profile below 500 m AGL, where observations are scarce and the PBL scheme can lead to errors. For each of the 41 far-inflow[A1] soundings from the 12 best sampled VORTEX2 supercells (5 nontornadic, 7 tornadic) in Parker (2014), a pseudosounding is created from the raw RUC gridded fields (i.e., not the SFCOA) for both the full resolution vertical grid and the pressure interpolated vertical grid. Similar to Coniglio (2012), to account for balloon drift, the gridded fields are interpolated to the time and location of the radiosonde along its path.

The average observed and RUC wind profiles for both the nontornadic and tornadic supercell cases are shown in Fig. A1, as well as the biases in SRH500. Although the shapes of the hodographs are fairly well represented, the winds below 500 m AGL are too fast in the RUC pseudosoundings (Figs. A1a,b), consistent

[A1] The far-inflow soundings are used here because their distance from the storm is less likely to entail convective contamination according to Potvin et al. (2010).

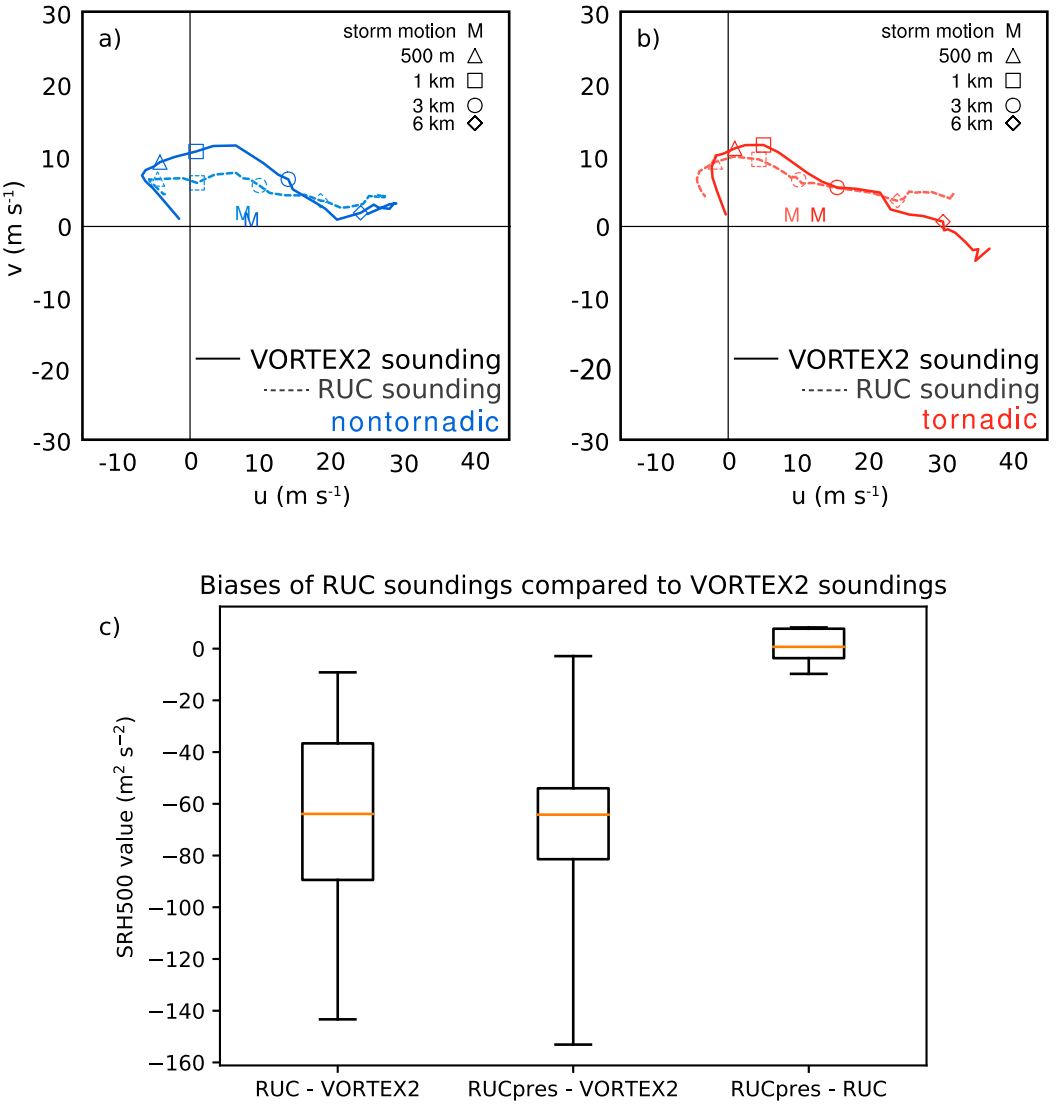

FIG. A1. (a),(b) Hodograph diagram comparing the average nontornadic (blue) and tornadic (red) wind profile for the 44 VORTEX2 far-inflow soundings (solid lines) from Parker (2014) with the average wind profile from the RUC pseudosoundings (faded dashed lines) for the same cases. (c) Box-and-whisker plot of biases in 0–500 m AGL SRH between the VORTEX2 far-inflow soundings and the RUC pseudosoundings, on both the full vertical resolution, native-level grid (RUC) and the vertical grid interpolated to 25-hPa increments (RUCpres). The storm motion in (a) and (b) is indicated on the hodograph by the "M". Markers on both hodographs represent 500 m (triangle), 1 km (square), 3 km (circle), and 6 km (diamond) AGL. See Parker (2014) for more discussion on the soundings that comprise these averages.

with Coniglio (2012). This is true regardless of the resolution of the model's vertical grid (Fig. A1c). This results in lowered near-ground SRH of 50–100 $m^2 s^{-2}$ (Fig. A1c). Near-ground SRH was especially underestimated in the tornadic environments (not shown). In addition to the loss of SRH, the CAngle is biased 20°–30° lower relative to the VORTEX2 sounding observations (not shown). These biases are a result of overmixed winds in the boundary layer and a change in the 10 m storm-relative inflow vector (one of the two components in the CAngle calculation). A plausible explanation for lack of CAngle values near 90° (as anticipated from the observations of Esterheld and Giuliano 2008) in the RUC soundings shown in Fig. 3 is that the RUC does not faithfully portray the wind profile in the PBL.

These comparisons between observed and model analyses have important ramifications to forecasters. Since very few severe weather events have optimal observed proximity soundings, forecasters rely on these analyses for operational awareness of the mesoscale

environment, especially above the surface where observations are particularly scarce. Although the RUC appears to struggle to represent the wind profile in the PBL (at least for these cases), the goal of the SPC's SFCOA scheme, which was applied to the all the proximity soundings discussed in sections 3 and 4, is to nudge the model forecast closer to reality using real-time surface data. Regardless, it is concerning that the underestimates of SRH appear to be more prevalent in environments that most strongly favor tornadoes (i.e., those with large lower-tropospheric shear). This means that, in reality, SRH500 probably has more skill than what is summarized here; unfortunately, in practice the forecaster must accept the skill that remains in the commonly available analysis products.

REFERENCES

Anderson-Frey, A. K., Y. P. Richardson, A. R. Dean, R. L. Thompson, and B. T. Smith, 2016: Investigation of near-storm environments for tornado events and warnings. *Wea. Forecasting*, **31**, 1771–1790, https://doi.org/10.1175/WAF-D-16-0046.1.

——, ——, ——, ——, and ——, 2017: Self-organizing maps for the investigation of tornadic near-storm environments. *Wea. Forecasting*, **32**, 1467–1475, https://doi.org/10.1175/WAF-D-17-0034.1.

Benjamin, S. G., and Coauthors, 2004: An hourly assimilation–forecast cycle: The RUC. *Mon. Wea. Rev.*, **132**, 495–518, https://doi.org/10.1175/1520-0493(2004)132<0495:AHACTR>2.0.CO;2.

——, and Coauthors, 2016: A North American hourly assimilation and model forecast cycle: The Rapid Refresh. *Mon. Wea. Rev.*, **144**, 1669–1694, https://doi.org/10.1175/MWR-D-15-0242.1.

Blumberg, W. G., K. T. Halbert, T. A. Supinie, P. T. Marsh, R. L. Thompson, and J. A. Hart, 2017: SHARPpy: An open-source sounding analysis toolkit for the atmospheric sciences. *Bull. Amer. Meteor. Soc.*, **98**, 1625–1636, https://doi.org/10.1175/BAMS-D-15-00309.1.

Bothwell, P., J. Hart, and R. Thompson, 2002: An integrated three-dimensional objective analysis scheme in use at the Storm Prediction Center. *21st Conf. on Severe Local Storms*, San Antonio, TX, Amer. Meteor. Soc., JP3.1, https://ams.confex.com/ams/SLS_WAF_NWP/techprogram/paper_47482.htm.

Bryan, G. H., J. C. Wyngaard, and J. M. Fritsch, 2003: Resolution requirements for the simulation of deep moist convection. *Mon. Wea. Rev.*, **131**, 2394–2416, https://doi.org/10.1175/1520-0493(2003)131<2394:RRFTSO>2.0.CO;2.

Bunkers, M. J., 2018: Observations of right-moving supercell motion forecast errors. *Wea. Forecasting*, **33**, 145–159, https://doi.org/10.1175/WAF-D-17-0133.1.

——, B. A. Klimowski, J. W. Zeitler, R. L. Thompson, and M. L. Weisman, 2000: Predicting supercell motion using a new hodograph technique. *Wea. Forecasting*, **15**, 61–79, https://doi.org/10.1175/1520-0434(2000)015<0061:PSMUAN>2.0.CO;2.

——, D. A. Barber, R. L. Thompson, R. Edwards, and J. Garner, 2014: Choosing a universal mean wind for supercell motion prediction. *J. Operational Meteor.*, **2**, 115–129, https://doi.org/10.15191/nwajom.2014.0211.

Caruso, J. M., and J. M. Davies, 2005: Tornadoes in nonmesocyclone environments with pre-existing vertical vorticity along convergence boundaries. *Electron. J. Operational Meteor.*, **6** (4), 1–36.

Clark, A. J., M. C. Coniglio, B. E. Coffer, G. Thompson, M. Xue, and F. Kong, 2015: Sensitivity of 24-h forecast dryline position and structure to boundary layer parameterizations in convection-allowing WRF Model simulations. *Wea. Forecasting*, **30**, 613–638, https://doi.org/10.1175/WAF-D-14-00078.1.

Coffer, B. E., 2016: Verification of RUC analyses using VORTEX2 soundings for nontornadic and tornadic supercell environments. *28th Conf. on Severe Local Storms*, Portland, OR, Amer. Meteor. Soc., 22, https://ams.confex.com/ams/28SLS/webprogram/Paper299924.html.

——, and M. D. Parker, 2015: Impacts of increasing low-level shear on supercells during the early evening transition. *Mon. Wea. Rev.*, **143**, 1945–1969, https://doi.org/10.1175/MWR-D-14-00328.1.

——, and ——, 2017: Simulated supercells in nontornadic and tornadic VORTEX2 environments. *Mon. Wea. Rev.*, **145**, 149–180, https://doi.org/10.1175/MWR-D-16-0226.1.

——, and ——, 2018: Is there a ''tipping point'' between simulated nontornadic and tornadic supercells in VORTEX2 environments? *Mon. Wea. Rev.*, **146**, 2667–2693, https://doi.org/10.1175/MWR-D-18-0050.1.

——, ——, J. M. Dahl, L. J. Wicker, and A. J. Clark, 2017: Volatility of tornadogenesis: An ensemble of simulated nontornadic and tornadic supercells in VORTEX2 environments. *Mon. Wea. Rev.*, **145**, 4605–4625, https://doi.org/10.1175/MWR-D-17-0152.1.

——, ——, and H. P. Taylor, 2018: Testing new environsmental proxies for supercell tornadogenesis using HRRR analyses. *29th Conf. on Severe Local Storms*, Stowe, VT, Amer. Meteor. Soc., 144, https://ams.confex.com/ams/29SLS/webprogram/Paper348555.html.

Cohen, A. E., 2010: Indices of violent tornado environments. *Electron. J. Oper. Meteor*, **11**, 2010-EJ6.

——, S. M. Cavallo, M. C. Coniglio, and H. E. Brooks, 2015: A review of planetary boundary layer parameterization schemes and their sensitivity in simulating southeastern U.S. cold season severe weather environments. *Wea. Forecasting*, **30**, 591–612, https://doi.org/10.1175/WAF-D-14-00105.1.

Coniglio, M. C., 2012: Verification of RUC 0-1-h forecasts and SPC mesoscale analyses using VORTEX2 soundings. *Wea. Forecasting*, **27**, 667–683, https://doi.org/10.1175/WAF-D-11-00096.1.

——, J. Correia Jr., P. T. Marsh, and F. Kong, 2013: Verification of convection-allowing WRF model forecasts of the planetary boundary layer using sounding observations. *Wea. Forecasting*, **28**, 842–862, https://doi.org/10.1175/WAF-D-12-00103.1.

Craven, J. P., H. E. Brooks, and J. A. Hart, 2004: Baseline climatology of sounding derived parameters associated with deep, moist convection. *Natl. Wea. Dig.*, **28**, 13–24.

Davies, J. M., 2004: Estimations of CIN and LFC associated with tornadic and nontornadic supercells. *Wea. Forecasting*, **19**, 714–726, https://doi.org/10.1175/1520-0434(2004)019<0714:EOCALA>2.0.CO;2.

Davies-Jones, R., 1984: Streamwise vorticity: The origin of updraft rotation in supercell storms. *J. Atmos. Sci.*, **41**, 2991–3006, https://doi.org/10.1175/1520-0469(1984)041<2991:SVTOOU>2.0.CO;2.

——, D. W. Burgess, and M. Foster, 1990: Test of helicity as a forecast parameter. Preprints, *16th Conf. on Severe Local Storms*, Kananaskis Park, AB, Canada, Amer. Meteor. Soc., 588–592.

Doswell, C. A., III, and D. M. Schultz, 2006: On the use of indices and parameters in forecasting severe storms. *Electron. J. Severe Storms Meteor.*, **1** (3), http://www.ejssm.org/ojs/index.php/ejssm/article/viewArticle/11/12.

——, R. Davies-Jones, and D. L. Keller, 1990: On summary measures of skill in rare event forecasting based on contingency tables. *Wea. Forecasting*, **5**, 576–585, https://doi.org/10.1175/1520-0434(1990)005<0576:OSMOSI>2.0.CO;2.

Emanuel, K. A., 1994: *Atmospheric Convection*. Oxford University Press, 592 pp.

Esterheld, J. M. and D. J. Giuliano, 2008: Discriminating between tornadic and non-tornadic supercells: A new hodograph technique. *Electron. J. Severe Storms Meteor.*, **3** (2), http://www.ejssm.org/ojs/index.php/ejssm/article/viewArticle/33.

Hampshire, N. L., R. M. Mosier, T. M. Ryan, and D. E. Cavanaugh, 2018: Relationship of low-level instability and tornado damage rating based on observed soundings. *J. Operational Meteor.*, **6**, 1–12, https://doi.org/10.15191/nwajom.2018.0601.

Hart, J. A., and W. Korotky, 1991: The SHARP workstation. NOAA/National Weather Service, 592 pp. [Available from NWS Eastern Region Headquarters, 630 Johnson Ave., Bohemia, NY, 11716.]

——, and A. E. Cohen, 2016: The challenge of forecasting significant tornadoes from June to October using convective parameters. *Wea. Forecasting*, **31**, 2075–2084, https://doi.org/10.1175/WAF-D-16-0005.1.

Johns, R. H., and C. A. Doswell III, 1992: Severe local storms forecasting. *Wea. Forecasting*, **7**, 588–612, https://doi.org/10.1175/1520-0434(1992)007<0588:SLSF>2.0.CO;2.

Knupp, K. R., and Coauthors, 2014: Meteorological overview of the devastating 27 April 2011 tornado outbreak. *Bull. Amer. Meteor. Soc.*, **95**, 1041–1062, https://doi.org/10.1175/BAMS-D-11-00229.1.

MacIntosh, C. W., and M. D. Parker, 2017: The 6 May 2010 elevated supercell during VORTEX2. *Mon. Wea. Rev.*, **145**, 2635–2657, https://doi.org/10.1175/MWR-D-16-0329.1.

Markowski, P. M., E. N. Rasmussen, and J. M. Straka, 1998a: The occurrence of tornadoes in supercells interacting with boundaries during VORTEX-95. *Wea. Forecasting*, **13**, 852–859, https://doi.org/10.1175/1520-0434(1998)013<0852:TOOTIS>2.0.CO;2.

——, J. M. Straka, and E. N. Rasmussen, 1998b: A preliminary investigation of the importance of helicity location in the hodograph. *19th Conf. on Severe Local Storms*, Minneapolis, MN, Amer. Meteor. Soc., 230–233.

——, C. Hannon, J. Frame, E. Lancaster, A. Pietrycha, R. Edwards, and R. L. Thompson, 2003: Characteristics of vertical wind profiles near supercells obtained from the Rapid Update Cycle. *Wea. Forecasting*, **18**, 1262–1272, https://doi.org/10.1175/1520-0434(2003)018<1262:COVWPN>2.0.CO;2.

Miller, D. J., 2006: Observations of low-level thermodynamic and wind shear profiles on significant tornado days. *23rd Conf. on Severe Local Storms*, St. Louis, MO, Amer. Meteor. Soc., 3.1, http://ams.confex.com/ams/pdfpapers/115403.pdf.

Monteverdi, J. P., C. A. Doswell III, and G. S. Lipari, 2003: Shear parameter thresholds for forecasting tornadic thunderstorms in northern and central California. *Wea. Forecasting*, **18**, 357–370, https://doi.org/10.1175/1520-0434(2003)018<0357:SPTFFT>2.0.CO;2.

Nowotarski, C. J., and A. A. Jensen, 2013: Classifying proximity soundings with self-organizing maps toward improving supercell and tornado forecasting. *Wea. Forecasting*, **28**, 783–801, https://doi.org/10.1175/WAF-D-12-00125.1.

——, P. M. Markowski, and Y. P. Richardson, 2011: The characteristics of numerically simulated supercell storms situated over statically stable boundary layers. *Mon. Wea. Rev.*, **139**, 3139–3162, https://doi.org/10.1175/MWR-D-10-05087.1.

Parker, M. D., 2014: Composite VORTEX2 supercell environments from near-storm soundings. *Mon. Wea. Rev.*, **142**, 508–529, https://doi.org/10.1175/MWR-D-13-00167.1.

Potvin, C. K., K. L. Elmore, and S. J. Weiss, 2010: Assessing the impacts of proximity sounding criteria on the climatology of significant tornado environments. *Wea. Forecasting*, **25**, 921–930, https://doi.org/10.1175/2010WAF2222368.1.

Rasmussen, E. N., 2003: Refined supercell and tornado forecast parameters. *Wea. Forecasting*, **18**, 530–535, https://doi.org/10.1175/1520-0434(2003)18<530:RSATFP>2.0.CO;2.

——, and D. O. Blanchard, 1998: A baseline climatology of sounding-derived supercell and tornado forecast parameters. *Wea. Forecasting*, **13**, 1148–1164, https://doi.org/10.1175/1520-0434(1998)013<1148:ABCOSD>2.0.CO;2.

Roebber, P. J., 2009: Visualizing multiple measures of forecast quality. *Wea. Forecasting*, **24**, 601–608, https://doi.org/10.1175/2008WAF2222159.1.

Sherburn, K. D., and M. D. Parker, 2014: Climatology and ingredients of significant severe convection in high-shear, low-CAPE environments. *Wea. Forecasting*, **29**, 854–877, https://doi.org/10.1175/WAF-D-13-00041.1.

Smith, B. T., R. L. Thompson, J. S. Grams, C. Broyles, and H. E. Brooks, 2012: Convective modes for significant severe thunderstorms in the contiguous United States. Part I: Storm classification and climatology. *Wea. Forecasting*, **27**, 1114–1135, https://doi.org/10.1175/WAF-D-11-00115.1.

——, ——, A. R. Dean, and P. T. Marsh, 2015: Diagnosing the conditional probability of tornado damage rating using environmental and radar attributes. *Wea. Forecasting*, **30**, 914–932, https://doi.org/10.1175/WAF-D-14-00122.1.

Stull, R. B., 1988: *An Introduction to Boundary Layer Meteorology*. Springer, 670 pp.

Thompson, R. L., and R. Edwards, 2000: An overview of environmental conditions and forecast implications of the 3 May 1999 tornado outbreak. *Wea. Forecasting*, **15**, 682–699, https://doi.org/10.1175/1520-0434(2000)015<0682:AOOECA>2.0.CO;2.

——, ——, J. A. Hart, K. L. Elmore, and P. Markowski, 2003: Close proximity soundings within supercell environments obtained from the Rapid Update Cycle. *Wea. Forecasting*, **18**, 1243–1261, https://doi.org/10.1175/1520-0434(2003)018<1243:CPSWSE>2.0.CO;2.

——, C. M. Mead, and R. Edwards, 2007: Effective storm-relative helicity and bulk shear in supercell thunderstorm environments. *Wea. Forecasting*, **22**, 102–115, https://doi.org/10.1175/WAF969.1.

——, B. T. Smith, J. S. Grams, A. R. Dean, and C. Broyles, 2012: Convective modes for significant severe thunderstorms in the contiguous United States. Part II: Supercell and QLCS tornado environments. *Wea. Forecasting*, **27**, 1136–1154, https://doi.org/10.1175/WAF-D-11-00116.1.

——, and Coauthors, 2017: Tornado damage rating probabilities derived from WSR-88D data. *Wea. Forecasting*, **32**, 1509–1528, https://doi.org/10.1175/WAF-D-17-0004.1.

Togstad, W. E., J. M. Davies, S. J. Corfidi, D. R. Bright, and A. R. Dean, 2011: Conditional probability estimation for significant tornadoes based on Rapid Update Cycle (RUC) profiles. *Wea. Forecasting*, **26**, 729–743, https://doi.org/10.1175/2011WAF2222440.1.

Wade, A. R., M. C. Coniglio, and C. L. Ziegler, 2018: Comparison of near- and fair-field supercell inflow environments using radiosonde observations. *Mon. Wea. Rev.*, **146**, 2403–2415, https://doi.org/10.1175/MWR-D-17-0276.1.

Webster, C., P. M. Markwoski, and Y. P. Richardson, 2014: What makes the sickle hodograph special? *27th Conf. on Severe Local Storms*, Madison, WI, Amer. Meteor. Soc., 3B.4A, https://ams.confex.com/ams/27SLS/webprogram/Paper254562.html.

Wicker, L. J., 1996: The role of near-surface wind shear on low-level mesocyclone generation and tornadoes. Preprints, *18th Conf. on Severe Local Storms,* San Francisco, CA, Amer. Meteor. Soc., 115–119.

Wilks, D. S., 2011: *Statistical Methods in the Atmospheric Sciences*. 3rd ed. International Geophysics Series, Vol. 100, Academic Press, 704 pp.

Wurman, J., D. Dowell, Y. Richardson, P. Markowski, E. Rasmussen, D. Burgess, L. Wicker, and H. B. Bluestein, 2012: The second Verification of the Origins of Rotation in Tornadoes Experiment: VORTEX2. *Bull. Amer. Meteor. Soc.*, **93**, 1147–1170, https://doi.org/10.1175/BAMS-D-11-00010.1.